The Helium–Neon Laser-Induced Fluorescence Spectrum of Molecular Iodine

An Undergraduate Laboratory Experiment

John S. Muenter
University of Rochester, Rochester, NY 14627

Lasers have made enormous contributions to experimental physical chemistry over the past two decades, but laser-based experiments in physical chemistry teaching laboratories are still relatively rare. There are many reasons for the slow appearance of lasers in course work; expense and complexity are two of the more obvious problems. This paper and the following one (*1*) describe two laser experiments that effectively introduce students to many of the advantages that lasers bring to studies of molecular spectroscopy and chemical kinetics. Both experiments use relatively affordable equipment and have very modest operating costs. These experiments join a rather small group of laser-based undergraduate laboratory projects (*2*), some of which are cited in ref *2*.

The first experiment, presented in this paper, is a high-resolution study of the helium–neon (He–Ne) laser-induced fluorescence spectrum of molecular iodine. The experimental results provide accurate values for B, ω_e, and $\omega_e x_e$ for the ground electronic state of I_2. From these spectroscopic properties, students calculate the bond length, harmonic-oscillator force constant, and a Birge–Sponer estimate of the bond-dissociation energy. The fluorescence spectrum exhibits both Stokes and anti-Stokes emissions, and clearly demonstrates the importance of Franck–Condon factors. The second experiment (*1*) uses a pulsed nitrogen laser to excite pyrene molecules, and observes the formation and decay of pyrene excimers.

He–Ne Laser-Induced Fluorescence

The He–Ne laser is the least expensive, simplest-to-operate, and most common laboratory laser. Many properties also make it well-suited as an excitation source for a wavelength-resolved fluorescence experiment. In particular, the He–Ne laser produces radiation having high spectral brightness and well-defined frequency. Its lack of tunability requires a coincidence between the radiation frequency and a molecular transition. The extremely dense visible-absorption spectrum of molecular iodine makes I_2 an ideal choice for He–Ne laser excitation.

Spectrum of Molecular Iodine

There are coincidences between He–Ne radiation and two different rotation–vibration electronic absorptions in I_2. The laser can excite $v'' = 3$, $J'' = 33$ of the ground electronic state to $v' = 6$, $J' = 32$ of the $B^3\Pi_{0u}^+$ electronic state, and also $v'' = 5$, $J'' = 127$ of the ground state to $v' = 11$, $J' = 128$ of the B state (*3*). These two transitions are referred to here as P(33)6←3 and R(127)11←5.

After excitation of the $v' = 6$, $J' = 32$ and $v' = 11$, $J' = 128$ energy levels of the B state, the excited molecules fluoresce back to the ground electronic state. The fluorescence obeys rigorous $\Delta J = \pm 1$ rotational selection rules, but the initially excited states can radiate to any vibrational level of the ground electronic state. The relative intensity of the fluorescence signals terminating on different v'' levels are determined by Franck–Condon factors or vibrational overlap integrals.

Fluorescence From the R(127)11←5 Excitation

Fluorescence arising from the R(127)11←5 excitation is described schematically in Figure 1. Most of the figure is taken up by the first twelve vibrational energy levels of the ground electronic state. There is not enough space to indicate even a few of the rotational energy levels supported by each vibrational state, but the specific rotational states involved in the laser-induced fluorescence transitions are shown for $v'' = 1$. The heavy upward arrow in the center of Figure 1 indicates the laser excitation from $v'' = 5$, $J'' = 127$.

The excitation terminates on $v' = 11$, $J' = 128$, indicated at the top of the figure. Emissions from the $v' = 11$, $J' = 128$ state come in closely spaced; $\Delta J = \pm 1$ pairs of lines go to each v'' level. The two transitions within each of these pairs terminate on $J'' = 127$ and $J'' = 129$, and are sepa-

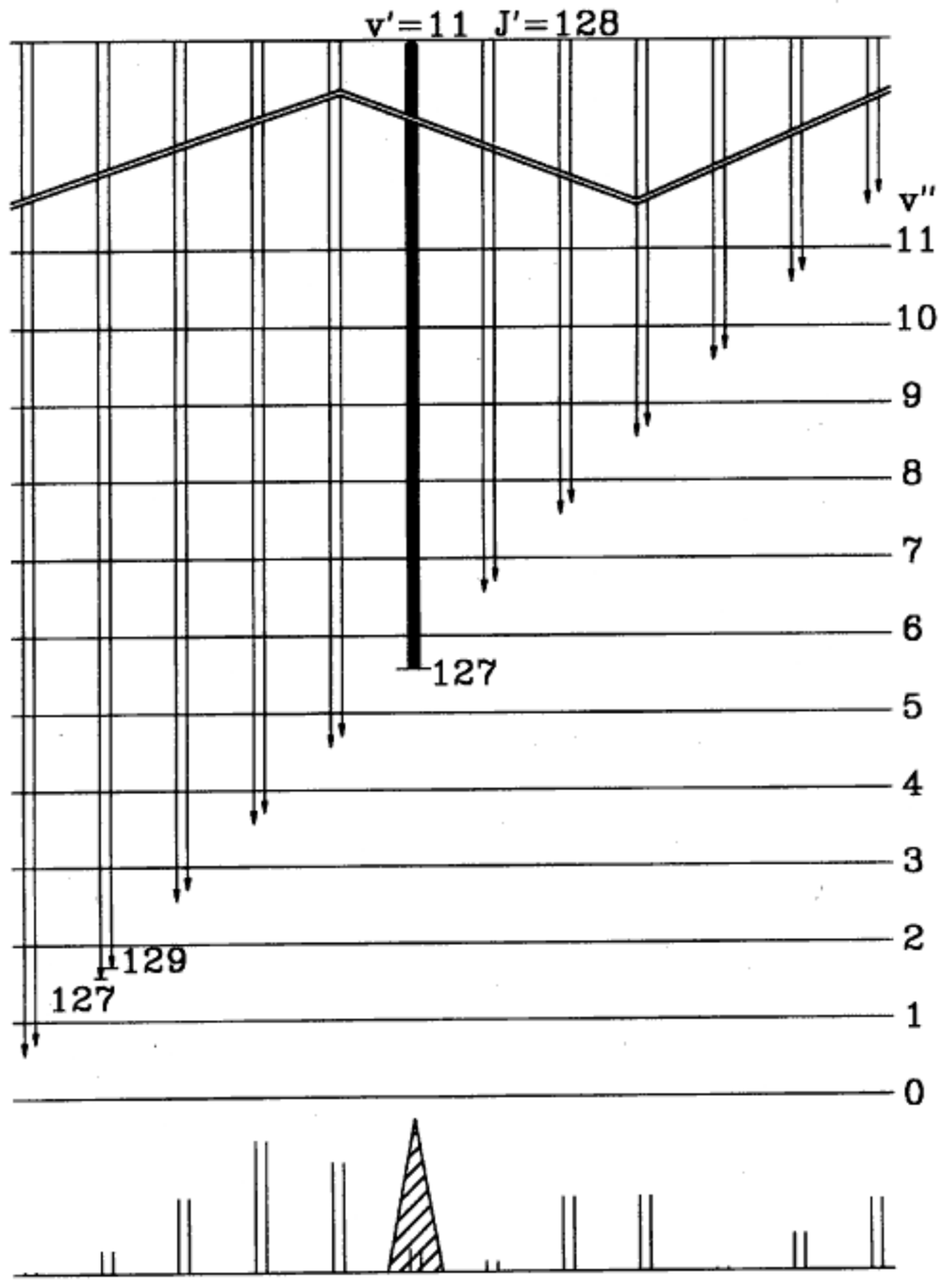

Figure 1. A schematic representation of the He–Ne laser excitation of the I_2 R(127)11←5 transition, and subsequent fluorescence.

Table 1. Franck–Condon Factors for He–Ne Excited I_2 Transitions[a]

	P(33) 6←3			R(127)11←5		
Δv	v'	v''	FCF[b]	v'	v''	FCF[b]
–5				11	0	2
–4				11	1	20
–3	6	0	0	11	2	68
–2	6	1	0	11	3	120
–1	6	2	3	11	4	100
0	6	3	21	11	5	20
1	6	4	55	11	6	9
2	6	5	100	11	7	68
3	6	6	120	11	8	68
4	6	7	83	11	9	2
5	6	8	2	11	10	33
6	6	9	0	11	11	65

[a]Data from ref *3*.

[b]Franck–Condon factors

rated by an energy of $514B \approx 20$ cm^{-1}. At 600 nm, $\Delta E \approx 20$ cm^{-1} corresponds to $\Delta\lambda \approx 0.8$ nm, and the rotational constant of I_2 can be measured with a monochromator of modest resolving power. The pairs of lines arising from the $\Delta J = \pm 1$ selection rules are separated by vibrational-energy-level spacings.

Relative intensities for the signals originating from $v' = 11$, determined by Frank–Condon factors listed in Table 1 (*3*) are indicated in a stick spectrum at the bottom of Figure 1. As shown, the intensities of the various signals vary greatly, and the experimental data clearly reflect this intensity distribution. The transitions ending on $v'' = 5$ are obscured by a large amount of scattered laser light, indicated by hash marks in Figure 1. Because the initial excitation is from an excited vibrational state, fluorescence signals occur at wavelengths both longer and shorter than the laser light. These signals are referred to as Stokes and anti-Stokes emissions.

Displacement of the Fluorescence from the Laser Frequency

The laser excites both $v' = 11$, $J' = 128$ and $v' = 6$, $J' = 32$; fluorescence from $v' = 6$ exhibits an entirely different set of relative intensities as indicated in Table 1. The Δv used to label the rows of Table 1 are defined as $v'' - v_{exc}$, where v'' identifies the state on which the fluorescence terminates, and v_{exc} is the state from which the laser excited the I_2 molecule. The Δv specifies the displacement of the fluorescence from the laser frequency, in units of I_2 vibrational-energy-level spacings. Positive Δv's indicate Stokes lines, and negative Δv's indicate anti-Stokes lines; $\Delta v = 0$ emissions occur at the laser frequency.

Because the rotational quantum numbers and the Franck–Condon factors are so different for the two sets of fluorescence transitions, they are easily distinguished. This is seen in Figure 2, which is a low-resolution recording of the He–Ne laser-induced fluorescence spectrum of I_2. The off-scale signal at 633 nm is scattered laser light, which obscures the $\Delta v = 0$ signal. The five anti-Stokes lines, labelled with their corresponding negative Δv's, all come from the R(127)11←5 excitation. The intensities of the five anti-Stokes signals nicely follow the Franck–Condon factors listed for the R(127)11←5 excitation.

The situation is not as simple for the Stokes signals.

- The $\Delta v = 1$ and $\Delta v = 4$ signals are dominated by fluorescence from $v' = 6$.
- The $\Delta v = 5$ and $\Delta v = 6$ signals are dominated by emission from $v' = 11$.
- The $\Delta v = 2$ and $\Delta v = 3$ signals contain significant contributions from both laser excitations.

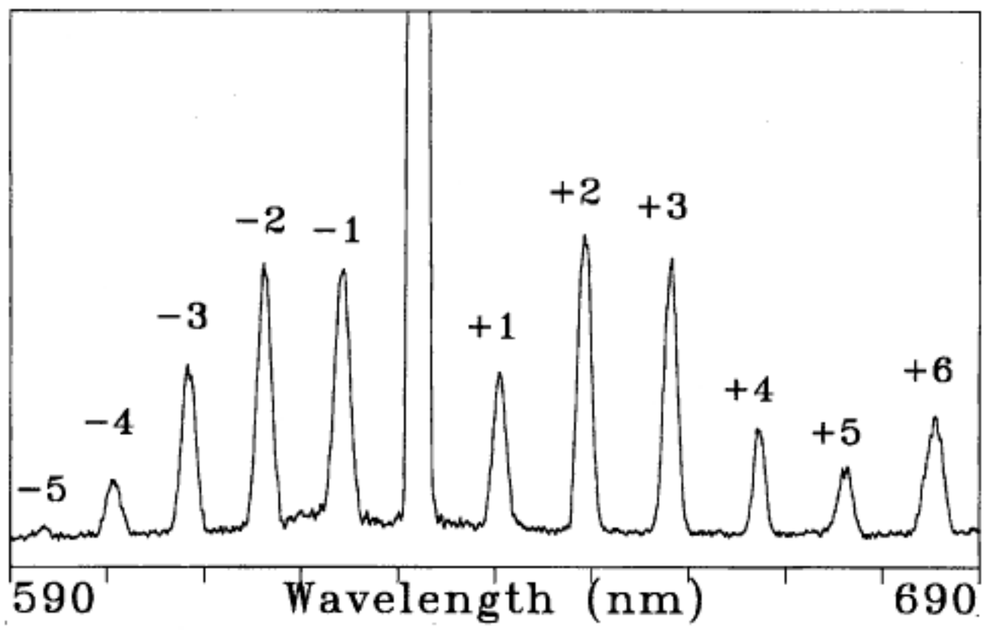

Figure 2. He–Ne laser-induced fluorescence spectrum of I_2 recorded with 1.25-nm resolution, using a PMT voltage of –800 and full-scale current sensitivity of 10 nA.

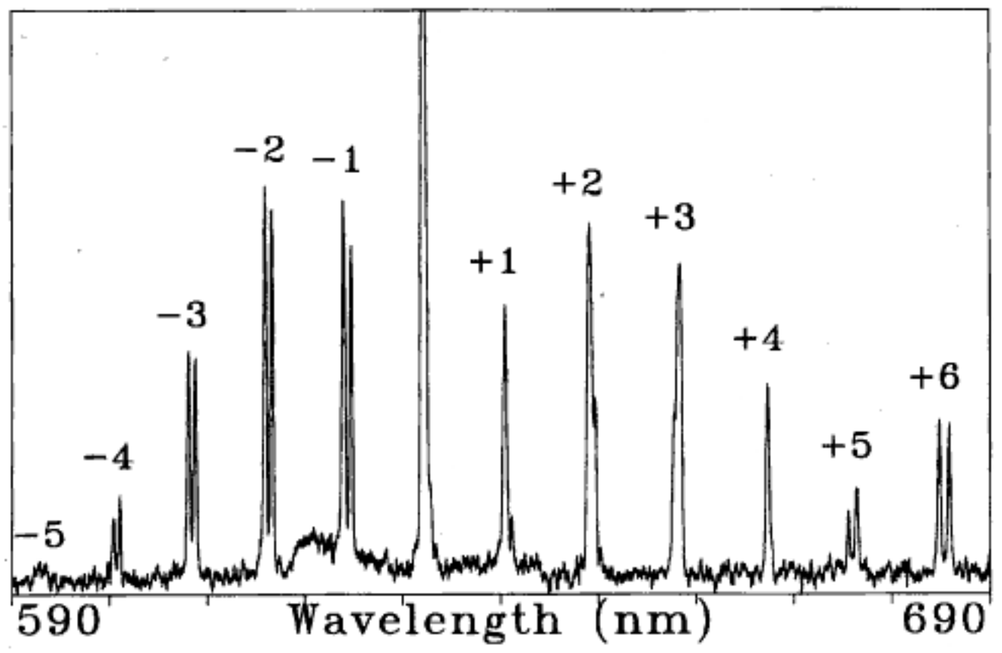

Figure 3. He–Ne laser-induced fluorescence spectrum of I_2 recorded with 0.25-nm resolution, using a PMT voltage of –800 and full-scale current sensitivity of 1 nA.

Higher-Resolution Spectrum

The validity of the Franck–Condon factors in Table 1 is nicely confirmed in the higher-resolution spectrum shown in Figure 3, recorded with 0.25-nm resolution. These data clearly resolve the separation of the signals terminating on $J'' = 127$ and $J'' = 129$, but cannot separate the much smaller splitting of the signals associated with $J'' = 31$ and $J'' = 33$. The $\Delta v = 1$ and $\Delta v = 4$ signals are clearly narrower than the composite signals from $\Delta v = 2$ and $\Delta v = 3$. Carefully recorded signals for $\Delta v = 2$ and $\Delta v = 3$, at 0.13-nm resolution, separate both sets of emissions. Figure 4 provides an expanded display of the $\Delta v = -2$ signal obtained with 0.25-nm resolution. The I_2 rotational constant and bond length are readily available from the information contained in this figure.

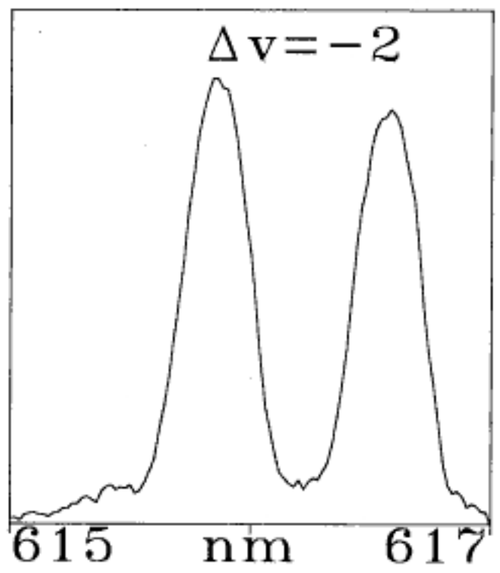

Figure 4. The $\Delta v = -2$ signal from Figure 2, expanded to show rotational resolution.

Relative Intensities

The Franck–Condon factors in Table 1 describe relative intensities for fluorescence signals from $v' = 6$ or $v' = 11$, but cannot be used to make comparisons between $v' = 6$ and $v' = 11$ signals. The intensities of signals from $v' = 6$, relative to those from $v' = 11$, depend on thermal populations of the $v'' = 3$ and $v'' = 5$ energy levels involved in the two excitations. They also depend on just how well the laser radiation overlaps the two absorptions. The importance of this second factor is made obvious by observing significantly different intensity distributions with different commercial He–Ne lasers.

Experimental Procedure

- ***Caution***: The laser beam is directed downward through the I_2 cell, so there is no possibility that students who lean over the apparatus can expose themselves to the *laser radiation*. It is important to stress laser safety to students, and information on this topic can be found in ref *2a*, pages 96 and 125.

Apparatus

Students have carried out this experiment in Rochester for many years, using several different sets of components. We have recently rebuilt the experiment, and this report is based on the new configuration. A block diagram for the experiment is shown in Figure 5. Table 2 lists manufacturers and model numbers for the specific components used. Over the years we have used three different He–Ne lasers with this experiment; two had output powers of 2 mW, and one had 5 mW. The figures shown here were obtained with the 5-mW laser. The main distinction between different lasers is the relative intensity of the $v' = 6$ vs. the $v' = 11$ emissions. Subtle differences in the spectral distribution affect how the laser radiation overlaps the P(33)6←3 and R(127)11←5 excitations.

Construction and Use of the I_2 Cell

The only necessary part of the experiment not commercially available is the I_2 cell. The cell is constructed from a 1-cm cuvette fitted with borosilicate glass tubulation rather than the usual stopper. The cuvette was evacuated on a simple vacuum manifold, and a small amount (less than 1 g) of I_2 was sublimed into the cell. The borosilicate glass tubulation was then sealed off under vacuum using a glassblowing torch. The effort invested in making a sealed I_2 cell is rewarded by many years of trouble-free service.

The cell is heated with Fiberglas-insulated heating tape that covers the central portion of the cuvette and tubulation. The cell is held horizontally (with a small three-finger clamp) with the "bottom" of the cuvette positioned close to the monochromator's entrance slits. The last half-centimeter of the cuvette is not covered by heating tape; this allows the laser beam to pass through the sample parallel to the monochromator slits. The monochromator slit assembly and the sample cell are covered with a piece of aluminum foil to keep the exposed end of the cuvette from being convectively cooled. A small hole in the foil allows the laser beam to reach the cell. The last centimeter of the tubulation is uncovered and not heated; this is the coolest part of the cell. This configuration insures that solid I_2 does not condense opposite the monochromator slits. The heating tape (a single-layer Thermoline/Briskheat B00051-020) is plugged into a variable transformer, but we use 115 V to heat the cell. The cell temperature is estimated to be about 70 °C.

Monochromator and Detector

Almost any small scanning monochromator can be used. As shown in Figure 2, useful vibrational information is available, even at low resolution. Rotational resolution can be obtained if a monochromator band pass of less than 0.5 nm is available. The monochromator used here is used without any scanning control or external interface. A TTL logic level determines the direction of the scan, and TTL pulses step the grating drive. The TTL pulses and logic level are obtained from a general purpose input/output (I/O) board installed in an IBM-compatible PC. This I/O board also contains the analog-to-digital converter used to digitize the fluorescence signal from the photomultiplier-tube (PMT) detector. The system is controlled by a data-acquisition program written in BASIC.

The PMT is the most critical component in the experiment due to the long wavelength and weak signals involved. High gain, good quantum efficiency at 700 nm, and low dark current are essential. We have used several different PMT's in this experiment, and the one listed in Table 2 is the only satisfactory choice found. Any side on, 1P28-type PMT housing is acceptable, although one with a shutter is convenient. It is necessary to carry out the experiment in a subdued light environment; you should either work in a room lit with a small incandescent lamp, or cover the laser, cell, and inlet slits of the monochromator with a dark cloth. Almost any regulated dc power supply capable of supplying up to –1000 V to the PMT is satisfactory. The current meter should be capable of measurements in the 1–10-nA range.

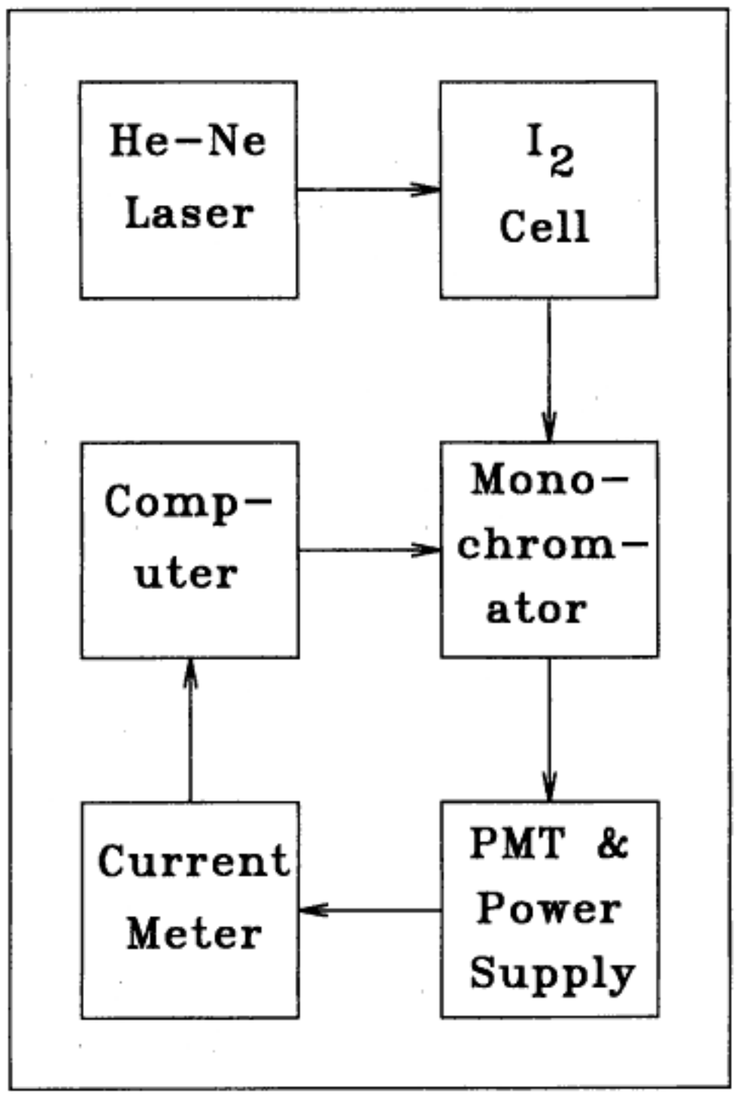

Figure 5. A block diagram for the He–Ne laser-induced fluorescence apparatus.

Table 2. Sources and Components Used

Component	Manufacturer	Model No.
Laser	Melles–Griot	05LLP851
Cell	NSG Precision Cells	63G
Monochromator	SPEX	340S
PMT	Hamamatsu	R928
PMT Housing	Products for Research	PR-1405 RF
PMT Power Supply	Hewlett–Packard	6515A
Current Meter	Keithley	410A
I/O Board	Metrabyte	DAS-1602

Procedure

This experiment can easily be completed in a single 3-h lab period, or it can be extended with additional projects to become a two-period assignment. The sample cell requires about 15 min to warm up, and during this time students familiarize themselves with the apparatus and the data-acquisition computer program. Then a series of short scans covering the $\Delta v = -2$ signal are carried out to optimize the position of the laser beam and to adjust the PMT voltage. The most accurate data are obtained by recording a single long scan of the spectrum, rather than recording a series of short segments. The PMT current, I, is recorded after each 0.02-nm wavelength step, so Figures 2 and 3 contain 5000 λ,I data points.

The large number of data are used to advantage in reducing noise by averaging adjacent points. Scans from 590 to 690 nm, as shown in Figures 2 and 3, are taken at several different monochromator slit widths. Narrower slit widths increase the resolution of the measurements but decrease the signal-to-noise ratio of the data. Students decide which spectrum will yield the most accurate results, and they analyze that data set.

Analysis

There are several different ways to analyze the data obtained in this experiment, and just one procedure is presented here. As a first step, the experimental λ,I data points are loaded into a commercial, computer-plotting, software package that features flexible data manipulation, data smoothing, and an active cursor used to measure the fluorescence peaks. Next, the spectrum is smoothed by averaging a number of adjacent data points. The number of points averaged is progressively increased until distortion of the spectrum is observed. Students then reduce the number of points averaged to obtain optimum smoothing. (Figures 2–4 have used seven-point averages.)

The observed wavelength of the scattered laser light, λ_{obs}(He–Ne), is then used to establish a monochromator calibration. $\Delta\lambda$ is defined as 632.82 – λ_{obs}(He–Ne), so the corrected wavelength, λ_{cor}, of any spectral feature is $\lambda_{cor} = \lambda_{obs} + \Delta\lambda$. Finally the spectrum is transformed from nanometers to inverse centimeters by replacing each λ value by $1/[(\lambda + \Delta\lambda)10^{-7}]$. A wavenumber value for each fluorescence peak associated with the R(127)11←5 excitation is measured from this smoothed, calibrated, and transformed spectrum.

We have chosen to first fit vibrational properties to the $v' = 11$, $J' = 128 \rightarrow v''$, $J'' = 127$ transitions. This choice allows using the He–Ne photon energy as a data point because the laser excitation corresponds to this signal for $\Delta v = 0$. The values (expressed in inverse centimeters) for these signals, $\bar{\nu}(v'')$, can be written (*4*)

$$\bar{\nu}(v'') = T_e + \omega'_e(11 + \tfrac{1}{2}) - \omega_e x'_e(11 + \tfrac{1}{2})^2 + B'128(129)$$

$$- \left(w''_e(v'') + \tfrac{1}{2}) - \omega_e x''_e(v'' + \tfrac{1}{2})^2 + B''127(128)\right)$$

$$= E_x + \omega''_e(v'' + \tfrac{1}{2}) - \omega_e x''_e(v'' + \tfrac{1}{2})^2$$

E_x in the second equality contains all of the energy terms that do not depend on v''. Least-squares fitting $\bar{\nu}(v'')$,v'' data pairs to w''_e and $w_e x''_e$ provides the desired I_2 vibrational properties. Table 3 lists v'', $\bar{\nu}(v'')$, and the $\bar{\nu}_{obs} - \bar{\nu}_{calc}$ obtained using the fitted values of $w''_e = 213.2(6)$ cm^{-1} and $w_e x''_e = 0.62(4)$ cm^{-1}.

The rotational constant comes from the $J'' = 127/129$ splittings. These are listed in Table 4 for several different v'' values. Clearly, these data are not sufficiently accurate to reflect any vibrational energy dependence of B; a simple average of these number gives $B'' = 0.0365(22)$ cm^{-1}. Standard expressions relate B, ω_e, and $\omega_e x_e$ to the bond length R, the harmonic-oscillator force constant k, and the bond-dissociation energy D_e. The results of $R = 2.79(8)$ Å, $k = 169.9(5)$ N/m, and $D_e \approx 18{,}000$ cm^{-1} are in excellent agreement with accepted values (*4*).

Table 3. I_2 Vibrational Data

v''	$\bar{\nu}(v'')$	Obsd–Calcd
1	16,639.1	–0.1
2	16,428.2	–0.2
3	16,220.1	1.2
4	16,010.3	–0.4
5	15,802.4	–1.3
7	15,395.3	1.9
8	15,189.1	–1.0
10	14,787.2	–0.1
11	14,587.9	0.1

Table 4. I_2 Rotational Data

v''	$\Delta\bar{\nu}(v'')$	Obsd–Calcd
1	19.1	0.3
2	18.7	–0.1
3	18.6	–0.2
4	19.1	0.3
7	17.9	–0.9
8	17.4	–1.4
10	18.2	–0.6
11	21.2	2.4

Discussion

This experiment closely parallels standard research techniques and generates high-quality data that students can analyze to obtain chemically important properties of the iodine molecule. The apparatus works well in student's hands, and there is very little frustration associated with data acquisition and analysis. This experiment also interacts constructively with the classic HCl IR vibration–rotation spectroscopy experiment and the study of the electronic absorption spectrum of I_2 (*5*). The work described here can also be extended in a number of different ways.

There are several additional transitions in the 690–770-nm region that are not assigned in the literature. Students can use the molecular properties determined here to assign these transitions, extend their data set, and carry out a more complete analysis. The calculation of Franck–Condon factors provides an excellent numerical project. This can be made relatively simple by using harmonic oscillator wave functions. Alternatively, more involved overlap integrals can be numerically evaluated using anharmonic wave functions. We combine this experiment with a Brewster's angle measurement and optical spectrum analysis of the He–Ne laser radiation.

The instrumentation uses standard techniques and is easy to set up. With some care, the entire experiment can be established for about $10,000. If a monochromator and computer are available, the cost can be less than half this amount. The basic apparatus can also be used to study atomic spectra, including the hydrogen Balmer series, alkali metal atom emissions, and the mercury spectrum. The same monochromator and photomultiplier detector are used in the nitrogen laser-induced chemical kinetics experiment described in the following paper (*1*). We also use

this monochromator and detector in a phosphorescence-lifetime experiment (*6*).

We provide our students with an extensive description of the experiment, including operating instructions and listings of the data-acquisition and data-analysis computer programs. Copies of this material, either on paper or WordPerfect 5.1 floppy disk, are available at no cost from the author.

Acknowledgment

Financial support from a Kresge Foundation grant is gratefully acknowledged.

Literature Cited

1. Muenter, J. S.; Deutsch, J. L. *J. Chem. Educ.* **1994**, 580–585 (the next paper).
2. (a.) Schwenz, R. W.; Moore, R. J. *Physical Chemistry: Developing a Dynamic Curriculum*; ACS: Washington, DC, 1993; Chapters 6–13; (b.) Galloway, D. B.; Clolkoowski, E. L.; Dallinger, R. F. *J. Chem. Educ.* **1992**, *69*, 79–83; (c.) Erskine, S. R.; Bobbit, D. R. *J. Chem. Educ.* **1989**, *66*, 354–357; (d.) Jones, B. T.; Smith, B. W.; Leong, M. B.; Mignardi, M. A.; Winefordner, J. D. *J. Chem. Educ.* **1989**, *66*, 357–358; (e.) King, M. E.; Pitha, R. W.; Soutum, S. F. *J. Chem. Educ.* **1989**, 66, 787–790; (f.) Hughes, E., Jr.; Jelks, V.; Hughes, D. L. *J. Chem. Educ.* **1988**, 65, 1007–1008.
3. Sakurai, K; Broida, H. P. *J. Chem. Phys.* **1970,** *53,* 1615–1616.
4. Herzberg, G. *Spectra of Diatomic Molecules*; van Nostrand: Princeton, 1950.
5. Shoemaker, D. P.; Garland, C. W.; Nibler, J. W. *Experiments in Physical Chemistry,* 5th ed.; McGraw–Hill: New York, 1989.
6. Dyke, T. R.; Muenter, J. S. *J. Chem. Educ.* **1975**, *52*, 251–258.

The Nitrogen-Laser Excited Luminescence of Pyrene

A Student Laboratory Study of Excimer Dynamics

John S. Muenter
University of Rochester, Rochester, NY 14627

John L. Deutsch
State University of New York, Geneseo, NY 14454

An undergraduate laboratory experiment that uses a nitrogen laser to produce the first excited singlet state of pyrene is described. The resulting luminescence is studied as a function of wavelength, time, and pyrene concentration to observe the dynamics of both the excited pyrene monomer and the pyrene excimer. The initial rise and subsequent decay of the excimer is directly observed. Data is analyzed in terms of coupled rate equations, and students obtain four different rate constants in interactive calculations. The apparatus is relatively easy to set up, and it introduces students to a variety of topics in photochemical kinetics and fast-measurement techniques.

The origins of physical chemistry were based on the need to understand the rates and mechanisms of chemical reactions. Investigating ever-faster processes is a continuing feature in the study of chemical kinetics and dynamics. In recent years, advances in lasers, electrooptics, and electronics have extended chemical measurements from nanosecond to femtosecond time regimes (*1*). Some of these same developments also make it perfectly feasible to observe nanosecond processes in undergraduate teaching laboratories. This paper describes the second of two student laboratory projects that introduce basic laser techniques into physical chemistry laboratories. The first of these two experiments (*2*) focuses on molecular spectroscopy and studies the rotationally resolved laser-induced fluorescence spectrum of molecular iodine. These two experiments join a relatively small group of laser-based undergraduate laboratory projects (*3*); some are cited in ref *3*. The present paper concentrates on fast kinetics measurements using a pulsed laser.

An ideal kinetics scheme for a student laboratory contains competitive first- and second-order reactions, and involves a reactive intermediate species. Monitoring the time and concentration dependence of reactants and products provides the necessary insight to understand both mechanisms and rates. The reaction dynamics of the first excited singlet state of pyrene provides these features, along with the advantages of laser initiation and optical detection. Students observe the time dependence of fluorescence from electronically excited pyrene and also from the pyrene excimer. Fluorescence signals, including those from the initial rise and then decay of the excimer concentration, are quantitatively measured and analyzed. The kinetic scheme is described by straightforward rate equations, but the coupling of these equations leads to moderately complicated time dependence of the chemical concentrations involved. In particular, students directly observe that not all radiative processes exhibit the simple exponential decay that results from first-order kinetics.

Pyrene: Its Luminescence and Excimer Formation

Pyrene is a planar aromatic hydrocarbon; its structure is shown in Figure 1. It is moderately soluble in common solvents, and the work described here is done in cyclohexane solution. The 337-nm radiation from a nitrogen laser excites the S_0 ground electronic state to the first excited singlet state, S_1. The resulting luminescence is quite intense and easily detected by eye, but this emission is not simple fluorescence (*4*).

Complex Radiative Decay

The complexity of pyrene's radiative decay is evidenced: It is both nonexponential in time and strongly concentration-dependent. Even simple visual inspection of the luminescence indicates unusual behavior. Emission from a 10^{-2} M pyrene solution is blue–green (peaking at about 500 nm), whereas a 10^{-6} M solution produces blue–violet emission (having a 390-nm maximum). These features suggest more than one active chemical species.

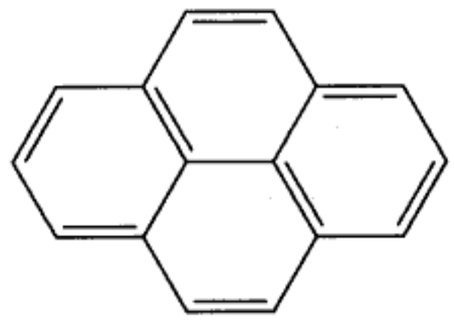

Figure 1. The structure of pyrene.